ACS APPLIED MATERIALS & INTERFACES

Research Article

www.acsami.org

Assessing the *in Vivo* Efficacy of Doxorubicin Loaded Hyaluronan Nanoparticles

Mohammad H. El-Dakdouki,*[,†,‡] Jingguang Xia,[‡] David C. Zhu,[§] Herbert Kavunja,[‡] Jessica Grieshaber,[‡] Sandra O'Reilly,[⊥,∥] J. Justin McCormick,[∥] and Xuefei Huang*[,‡]

[†]Department of Chemistry, Beirut Arab University, P.O. Box 11-5020 Riad El Solh 11072809, Beirut, Lebanon

[‡]Department of Chemistry, Michigan State University, Chemistry Building, Room 426, 578 South Shaw Lane, East Lansing, Michigan 48824, United States

[§]Departments of Radiology and Psychology, Michigan State University, East Lansing, Michigan 48824, United States

[∥]Carcinogenesis Laboratory, Department of Microbiology & Molecular Genetics, Michigan State University, East Lansing, Michigan 48824, United States

[⊥]Research Technology and Support Facility, Imaging-IVIS, Biomedical and Physical Sciences Building, Michigan State University, East Lansing, Michigan 48824, United States

Supporting Information

ABSTRACT: Magnetic nanoparticles are attractive platforms for biomedical applications including diagnosis and treatment of diseases. We have shown previously that hyaluronan-coated superparamagnetic iron oxide nanoparticles (HA-SPIONs) enhanced the efficacy of the conjugated anticancer drug doxorubicin (DOX) *in vitro* against drug-sensitive and drug-resistant human ovarian cancer cells. In this manuscript, we report our findings on the efficacy of DOX loaded HA-SPIONs *in vivo* using subcutaneous and intraperitoneal SKOV-3 ovarian tumor models in nude mice. The accumulation of the nanoparticles in subcutaneous tumors following an intravenous nanoparticle administration was confirmed by magnetic resonance imaging, and its distribution in the tumors was evaluated by confocal microscopy and Prussian blue staining. DOX delivered by nanoparticles accumulated at much higher levels and distributed wider in the tumor tissue than intravenously injected free DOX, leading to significant reduction of tumor growth. The IVIS Spectrum for *in vivo* bioluminescence imaging was used to aid in therapy assessment of the DOX-loaded nanoparticles on intraperitoneal ovarian tumors formed by firefly luciferase expressing human ovarian SKOV-3 cells. DOX-loaded HA-SPIONs significantly reduced tumor growth, delayed tumor development, and extended the survival of mice. Thus, utilizing HA-SPIONs as drug delivery vehicles constitutes a promising approach to tackle CD44 expressing ovarian cancer.

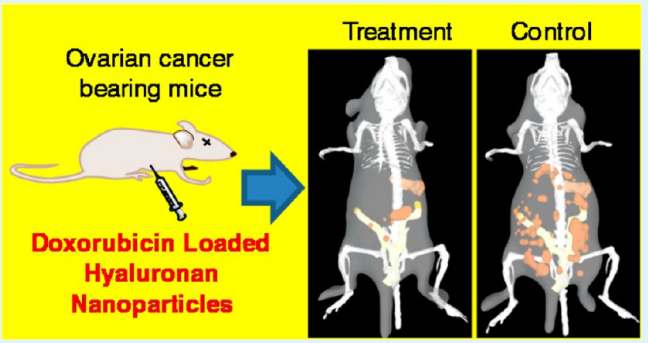

KEYWORDS: *CD44, doxorubicin, drug delivery, hyaluronan, magnetic nanoparticles, ovarian cancer*

INTRODUCTION

Ovarian cancer is the fifth most common form of cancer among American women, and the leading cause of death from gynecological malignancies. An estimated 22 240 new cases of ovarian cancer are expected to be diagnosed in the USA in 2013 with an estimated 14 030 deaths.[1] The majority of early diagnosed ovarian cancer cases (~95%) are likely to be cured by optimal surgical debulking of the primary tumor followed by a carboplatin−paclitaxel combination treatment.[2,3] However, 75% of women with ovarian cancer are diagnosed at an advanced stage of the disease when there is little hope of cure.[4] This is because symptoms, such as bloating, pelvic, or abdominal pain, associated with early ovarian cancer when it is still limited to the ovaries are nonspecific and similar to those associated with common gastrointestinal, genitourinary, and gynecological conditions.[5,6] In addition, the initial high response rate of 80% to chemotherapy does not translate into improved overall patient survival rate due to the relapse of the disease and the development of drug resistance against platinum-based therapies.[7] Chemotherapeutic agents such as liposomal doxorubicin (Doxil),[8] topotecan,[9] gemcitabine,[10] and tamoxifen[11] are used in the cases of platinum-refractory relapsed ovarian cancer.[12] Currently, there is an unprecedented interest in exploiting molecular targeted therapy to overcome drug resistance. In this regard, a large number of novel agents targeting angiogenesis, DNA repair, human epidermal growth factor receptors (EGFR), and estrogen receptors are undergoing clinical trials.[4,13−16]

Received: November 5, 2013
Accepted: December 5, 2013
Published: December 5, 2013

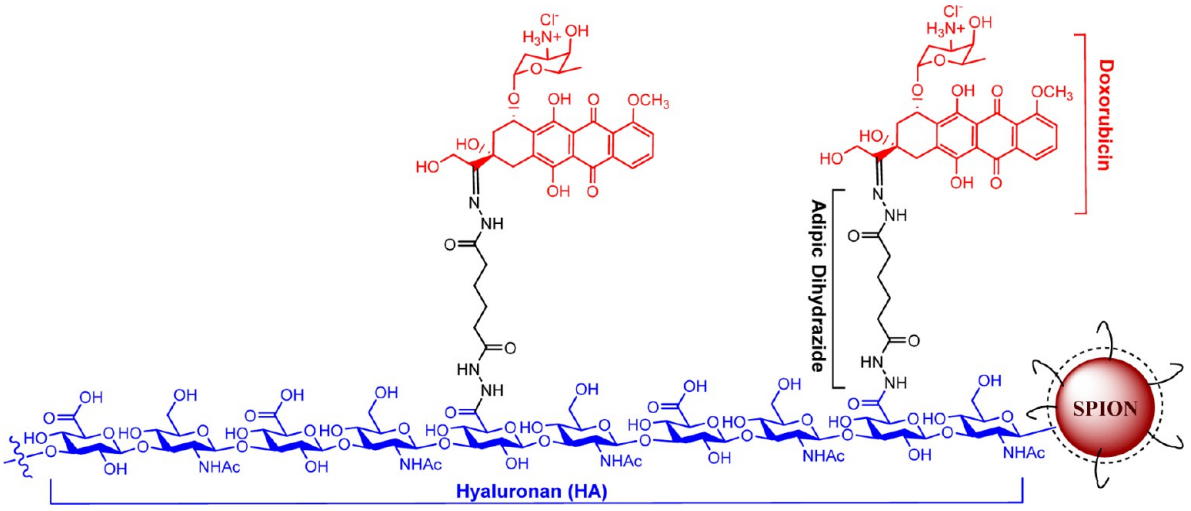

Figure 1. Doxorubicin-loaded, hyaluronan-coated superparamagnetic iron oxide nanoparticle (DOX-HA-SPION). For detailed synthesis and characterization of the nanoparticles, please refer to ref 27. Note that the figure is not drawn to scale.

Nanotechnology has emerged as a powerful tool for drug delivery,[17,18] imaging,[19] therapy assessment,[20,21] and circumventing multidrug resistance.[22−24] We are interested in the development of magnetic nanoparticles for biological applications including cell labeling,[25] pathogen detection and decontamination,[26] cancer differentiation,[27,28] atherosclerosis,[29−31] and Alzheimer's disease detection.[32] Owing to their biocompatibility,[33] superparamagnetic iron oxide nanoparticles (SPIONs) have been extensively utilized as drug delivery vehicles[34] as well as magnetic resonance imaging (MRI) contrast agents.[35,36] Drugs delivered by iron oxide nanoparticles were found to reverse drug resistance in several cancer cell lines[37−39] including ovarian cancer.[40] We recently reported that conjugating the anticancer drug doxorubicin (DOX) on the surface of nanoparticles (Figure 1) rendered the DOX-resistant NCI-ADR-RES ovarian cancer cells more sensitive to drug treatment most likely through modulation of the intracellular distribution of drug.[27] The interaction between the hyaluronan (HA) coating on the nanoparticles and the CD44 receptor overexpressed on the external cell membranes of SKOV-3 epithelial ovarian cancer cells facilitated the enhanced uptake of the nanoparticles by cells in 2D cell cultures,[41] and mediated deeper penetration of the nanoparticles in 3D SKOV-3 cancer spheroids through receptor mediated transcytosis.[42] In this manuscript, we investigate the efficacy of DOX conjugated onto HA-SPIONs *in vivo* in subcutaneous (S.C.) and intraperitoneal (I.P.) mice tumor models, and examine the distribution of DOX within the tumor tissue.

EXPERIMENTAL SECTION

Materials and Instrumentation. All chemicals were reagent grade and were used as received from the manufacturers. Fetal bovine serum (FBS), neutral fast red, and 10% neutral formalin solution were purchased from Sigma-Aldrich. FBS was inactivated by heating at 60 °C for 30 min. Doxorubicin hydrochloride was purchased from Shanghai FChemicals Technology Co. The SKOV-3 cell line was purchased from American Type Culture Collection (ATCC). Phosphate buffered saline (PBS), Dulbecco's modified eagle medium (DMEM), sodium pyruvate (100 mM), glutamine, penicillin−streptomycin (pen−strep) mixture, and blasticidin were purchased from Invitrogen. D-Luciferin was obtained from Promega. Synthetic mounting medium (MM24) was obtained from SelecTech. Pre-made firefly luciferase (luc) lentiviral particles (EF1a-luciferase (firefly)-2A-RFP (blasticidin)), expressing luciferase II gene under re-engineered EF1a promoter which also co-expressed RFP marker, was purchased from GenTarget Inc (catalogue number: LVP439). All cell culture growth media was supplemented with 10% inactivated FBS, 1% pen−strep mixture, glutamine (2 mM), and sodium pyruvate (1 mM). The SKOV-3 cell line was cultured in DMEM and maintained in a CO_2 incubator set at 37 °C. Cell sorting was performed on a BD Influx Cell Sorter. Fluorescence images were acquired on a Nikon Eclipse TE2000-U microscope. Confocal laser microscopy images were collected on an Olympus FluoView 1000 LSM confocal microscope. DOX-HA-SPIONs were synthesized as described previously,[27] and purified by gel permeation chromatography to remove any free DOX prior to treatment. The amount of DOX on the nanoparticles was quantified by UV-vis measurements carried out on a UV-4001 spectrometer (Hitachi High-Technologies Co., Japan). All animal experiments were in accordance with the policies, guidelines, and approval of Michigan State University's Institutional Animal Care and Use Committee (IACUC). Six weeks old athymic female nude Balb C mice were bred and housed in Innovive cages with free access to water and chow in a specific pathogen free (SPF) facility adjoining the IVIS Spectrum imaging room.

MRI of Mice. Mice bearing S.C. SKOV-3 tumors (see below for tumor growth) were anesthetized with ketamine (35 mg/kg, i.p.) and xylazine (5 mg/kg, i.p.). MR images were acquired on a clinical 3T GE MRI scanner prior to nanoparticle injection. HA-SPIONs (40 mg of NP/mL, 25 μL) were then injected intravenously (via tail vein), and the mice were imaged 1, 2, and 24 h post injection. Areas rich in SPIONs display negative (black) contrast in the images. The following parameters were used to evaluate the T_2* effect of the uptake of the nanoparticles: wrist coil, 3D fast spoiled gradient recalled echo sequence, flip angle = 15°, echo time (TE) = 10.6 ms, time of repetition (TR) = 21.6 ms, receiver bandwidth (rBW) = ±7.8 kHz, field of view (FOV) = 4 cm, slice thickness = 1 mm, number of slices = 36, acquisition matrix = 256 × 256, frequency direction = anterior/posterior, number of excitation (NEX) = 4, and scan time = 13 min 15 s.

Subcutaneous Ovarian Tumor Model. Female athymic nude mice were injected subcutaneously with 4×10^6 SKOV-3 cells on the right flank, and tumors were allowed to grow over a period of 5 weeks. The body weight of the mice was routinely measured, and the mice were monitored for any adverse health effects. A digital caliper was used to determine the tumor dimensions. The volume of the tumors was determined using the following formula: volume (cm^3) = 0.523 (d1 × d2 × d3), where d1, d2, and d3 represent measurements in each of the three dimensions of the tumor (i.e., length, width, and thickness). Mice which developed a tumor 0.5 cm^3 in volume or 1 cm in any of the three dimensions were euthanized. On week 5 following

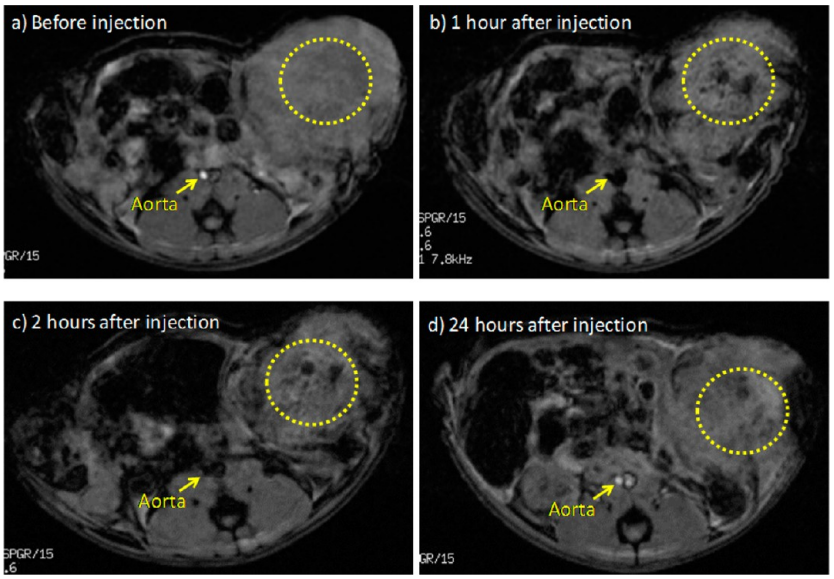

Figure 2. *In vivo* T_2*-weighted MR images of mouse tumor: (a) before injection, (b) 1 h, (c) 2 h, and (d) 24 h after HA-SPION injection (1 mg-NP/kg of body weight). The negative contrast (darkening) highlighted in the yellow circle suggested the presence of SPION.

injection of SKOV-3 cells, the mice were randomly divided into three groups and injected intravenously with either vehicle (PBS), 1 mg of DOX/kg of free DOX, or 1 mg of DOX/kg conjugated to nanoparticles. The mice received six injections over the course of 2 weeks. During the course of treatment, the percentage of tumor growth was determined using the following formula: % tumor growth = (volume of tumor during treatment/volume of tumor prior to treatment) × 100. At the end of the study, the mice were euthanized. During necropsy, tumors were collected, and *ex vivo* DOX fluorescence was measured in tumors using the LivingImage software of the IVIS Spectrum.

Histological Studies. Following fluorescent imaging, excised tumors were embedded in optimal cutting temperature (OCT) solution without fixing, and frozen using a dry ice/ethanol solution. Thin cryosections (7 μm thickness) were collected on charged glass slides, and stored at −80 °C. Stored sections were removed from the −80 °C freezer and allowed to reach room temperature 1 h before experiments. To visually confirm the presence of DOX in the tumor, sections were fixed with 10% neutral buffered formalin solution. Sections were air dried in the dark, mounted with synthetic mounting media, and stored in the dark for confocal imaging.

Prussian Blue Staining. Frozen sections were removed from the −80 °C freezer and allowed to reach room temperature 1 h before preparation for staining. Tissues were immersed in 10% potassium ferrocyanide trihydrate ($K_4Fe(CN)_6{\cdot}3H_2O$) solution for 10 min, followed by a 1:1 solution of 10% potassium ferrocyanide trihydrate ($K_4Fe(CN)_6{\cdot}3H_2O$) and 20% HCl solutions for 30 min. The sections were washed in PBS, counterstained with neutral fast red, and then washed with double distilled water. Sections were dehydrated by serial dilutions in ethanol (25, 50, 75, and 100%) followed by xylene treatment. The sections were mounted and covered with a coverslip. Images were collected using an inverted light microscope.

Transfection of the SKOV-3 Cancer Cells with Luciferase. SKOV-3 cancer cells (5×10^4 cells in 500 μL growth media) were seeded in a 24-well plate. At 50% confluency, the cells were washed three times with PBS, and 50 μL of the lentivirus stock (EF1a-luciferase (firefly)-2A-RFP (blasticidin)) in 450 μL growth medium was added to the cells. The cells were incubated at 37 °C and 5% CO_2 for 72 h, and selected using blasticidin. Cells that received growth media only were used as a negative control. To confirm the successful expression of the gene, the cells were imaged for RFP expression using a fluorescence microscope. Since the RFP signal was not uniform throughout the culture, cells were sorted by flow cytometry. Cells that yielded the highest RFP fluorescence were collected and cultured in complete growth medium. To determine the limit of detection of the cells for bioluminescence and fluorescence imaging using the IVIS Spectrum, cells were serially diluted (200×10^3, 100×10^3, 50×10^3, 25×10^3, and 12.5×10^3 cells) and seeded on a 96-well black-walled, clear bottomed plate. 96-well plate quantification allows the use of bioluminescence and fluorescence tomography to determine not only the depth and anatomical location of the source in an animal but extrapolation of the intensity of the bioluminescent or fluorescent signal to the number of cells or dye molecules in the signal source. Fluorescent images of the plate were first collected on the IVIS Spectrum, and fluorescence intensity was determined and plotted against the number of cells to confirm linearity. D-Luciferin (300 μg/mL, 100 μL) was then added to the cells, and the plate was incubated for 5 min. Bioluminescence images were collected, and bioluminescence intensity was determined and plotted against the number the cells. The transfected SKOV-3-Luc cells were used in subsequent *in vivo* experiments.

Intraperitoneal Ovarian Cancer Model. Athymic nude mice were injected I.P. with SKOV-3-Luc cells (1×10^6 cells/mouse) and divided randomly into three treatment groups (vehicle [PBS] only, free DOX [2 mg/kg], and DOX conjugated onto SPION). Mice were treated I.P. three times per week for a period of 4 weeks, after which treatment was halted and the progress of the disease was monitored. Bioluminescence images were collected the day after cell injection and weekly throughout the study. Prior to imaging for bioluminescence, mice were injected I.P. with D-luciferin (150 mg/kg). Bioluminescence images were analyzed using the LivingImage processing software. Regions of interest (ROIs) were drawn around the bioluminescent signals in the abdominal area of the mice, and measurements were automatically generated as integrated flux of photons (photons/s) by the LivingImage processing software. The abdomen size was measured using a digital caliper, and the weight of the mice was determined on a digital scale. Following euthanasia, mice were necropsied for pathological examination.

RESULTS AND DISCUSSION

Targeting Ability, Efficacy, and Distribution of DOX-HA-SPIONs in the Subcutaneous Tumor Model. Having demonstrated previously that HA enhanced the penetration potential of nanoparticles in 3D cancer spheroids through receptor mediated transcytosis,[42] and that DOX immobilized on HA-coated nanoparticles exhibited improved efficacy *in vitro*,[27,41] we set out to test our findings *in vivo* in two tumor

models. We have shown in several studies that HA-SPIONs are colloidally stable and biocompatible,[27,29,31] and safe when evaluated in rabbit models.[29] We started the *in vivo* validation process by subcutaneously growing SKOV-3 tumors in the right flank of athymic nude female mice. First, we wanted to confirm that HA-SPION can efficiently accumulate in the tumor possibly by a combination of passive targeting through the enhanced permeability and retention (EPR) effect and active targeting due to the binding of the HA coating to the CD44 receptors overexpressed on SKOV-3 cells.[27] The high magnetic moments of SPIONs induce inhomogeneity in the local magnetic field by shortening the transverse relaxation (T_2*) of nearby water protons, causing signal loss and darkening in T_2- and T_2*-weighted MR images.[43] We have shown previously that HA-SPIONs exhibited high relaxivities (r_2* value = 361 mM^{-1} s^{-1} at 3 Tesla), and served as effective negative MRI contrast agents enabling the *in vivo* imaging of atherosclerotic plaques.[29] In the current study, we monitored the accumulation of nanoparticles in tumors by MRI. Mice were injected with HA-SPION via tail vein, and images were collected pre-injection and at 1, 2, and 24 h post-injection on a clinical 3T MR scanner. While no darkening was observed in either the tumor mass or the aorta lumen prior to injection (Figure 2a), major darkening was detected 1 h (Figure 2b) and 2 h (Figure 2c) following nanoparticle injection. To confirm that the detected darkening in the tumors was not due to SPIONs circulating in the blood vessels (blood pool effect), MRI was performed 24 h post-injection to allow for clearance of the nanoparticles from the circulation (Figure 2d). The aorta lumen appeared bright at 24 h, indicating the clearance of nanoparticles from the blood pool. Darkening persisted in the tumors, demonstrating the accumulation of nanoparticles in the tumor. These results highlight the advantage of HA-SPIONs, which can be used to non-invasively monitor the delivery process.

To evaluate the efficacy and tumoral distribution of free DOX and DOX delivered by HA-SPION, mice were randomly divided into three groups: vehicle control group (PBS only), a group that received the anticancer drug doxorubicin at a concentration of 1 mg-DOX/kg-animal body weight, and a group that was treated with an equivalent amount of DOX conjugated to HA-SPION. The mice received three injections weekly for 2 weeks (total of six injections). During the 6-week duration of the study, the mice were monitored for any adverse health effects due to the treatment, showing no signs of toxicity or fatigue. The percentage of tumor growth was determined with respect to the tumor volume prior to the first treatment. The tumors in the vehicle (PBS) control group grew to an average of 180% in size (Figure 3). When DOX was administered in its free form, it did not reduce the size of the tumor much, as revealed by the 140% increase in tumor size. On the other hand, DOX-loaded nanoparticles inhibited the growth of the tumors compared to the control group with an average of only 45% increase in tumor size (Figure 3).

The improved antitumor activity of DOX-HA-SPION can be rationalized by the ability of the nanocarrier to modulate the pharmacodynamic and pharmacokinetic properties of the drug. Free DOX has a short half-life of 10 min.[44,45] In comparison, DOX-loaded nanoparticles circulated the blood pool for at least 3 h, as revealed by the MRI images (Figure 2), allowing for substantial accumulation in the tumor. In addition, it has been shown that increasing the molecular weight of the carrying polymer increased tumoral accumulation while reducing renal

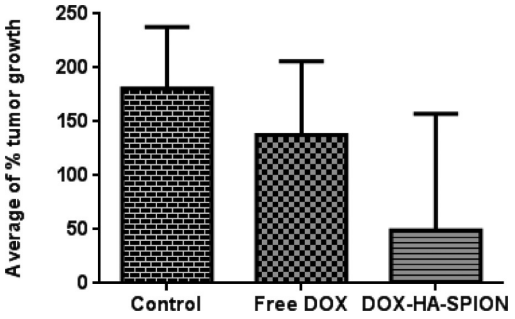

Figure 3. Percentage of tumor growth in control, free DOX-treated, and DOX-HA-SPION-treated mice. The tumor size at the day of first treatment was used as the reference.

clearance.[44] Thus, conjugating DOX to a nanoparticle can lead to delivery of higher cytotoxic doses of the drug, which translates to a better therapeutic outcome. To support this hypothesis, whole tumors were excised and imaged using the IVIS Spectrum for DOX fluorescence. While the group treated with free DOX showed 2 times the DOX fluorescence inside the tumor compared to the untreated group, the levels of DOX in tumors from nanoparticle-treated mice were 30 times higher than the control untreated group, suggesting much higher amounts of DOX accumulated in the tumor when delivered by the nanoparticles (Figure 4).

It has been demonstrated by Tannouk et al. that the inability of weakly basic drugs such as DOX to penetrate solid tumors leads to non-uniform distribution of drugs in the tumor tissue, which is a potential mechanism for drug resistance.[46,47] In an attempt to improve the penetration and distribution of DOX in tumors, we recently reported that HA-coated silica nanoparticles enhanced the delivery of DOX deep in the tumor through CD44 mediated transcytosis, resulting in increased cytotoxicity against SKOV-3 ovarian cancer spheroids.[42] To validate our findings *in vivo*, tumor sections were imaged on a confocal microscope by exploiting the intrinsic red fluorescence of DOX. As expected, no DOX fluorescence was detected in sections collected from tumors of the control (PBS only) mice (Figure 5a). Whereas the signal due to DOX was scarce in the tumors of mice treated with free DOX (Figure 5b), the DOX signal was much more abundant in tumors when DOX was delivered by SPIONs (Figure 5c). Quantitative analysis of the images showed that the fluorescence of DOX was 16-fold higher in the tumor sections collected from mice treated with DOX-HA-SPIONs as compared to the ones receiving free DOX (Figure 5d). In addition, measuring the areas of the sections where DOX was detected revealed that DOX from nanoparticles covered 34 times greater area than free DOX (Figure 5e), highlighting the value of using the nanoparticle platform to achieve a better distribution of poorly penetrating drugs in tumors. This may account in part for the improved efficacy observed in the mice treated with DOX conjugated to nanoparticles.

To co-register the presence of DOX with that of the nanoparticles, Prussian blue staining, which is selective for ferric ions, was performed on the tumor sections. Iron ions, which appeared as blue stains in Figure 6a, appeared in the same regions as the red fluorescent DOX (Figure 6b). These observations highlight the significance of the HA-coated SPION as an efficient drug delivery vehicle that can augment the accumulation and retention of drugs in the tumors.

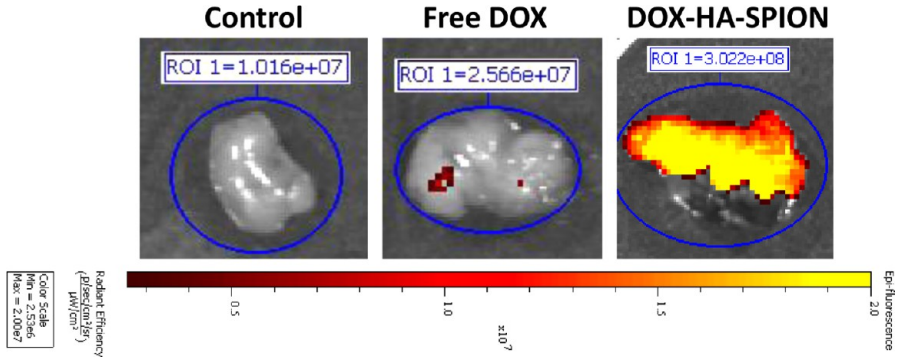

Figure 4. *Ex vivo* fluorescence images of representative tumors captured on the IVIS system. The region of interest (ROI) was drawn around tumors, and radiant efficiency measurements were automatically assigned by the LiveImage software used for image processing. HA-SPIONs significantly improved the delivery of DOX to the tumors.

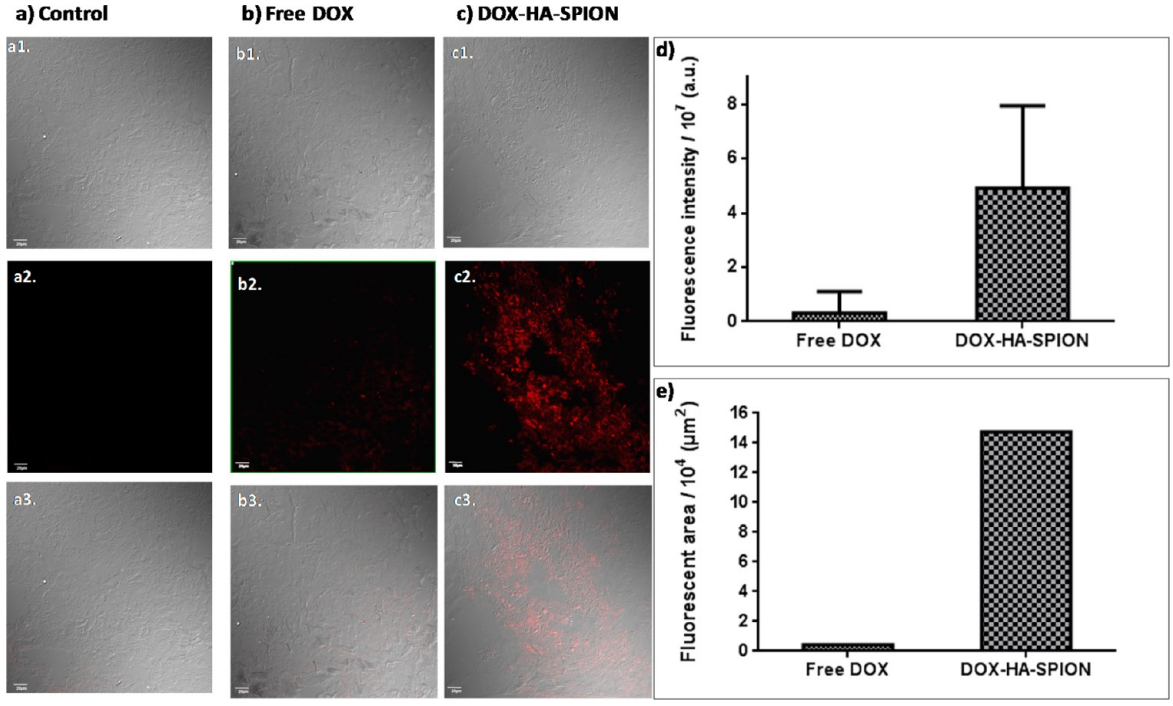

Figure 5. Laser confocal microscopy images collected for tumor sections from control (a), free DOX-treated (b), and DOX-HA-SPION-treated mice (c). (a1, b1, c1) DIC images; (a2, b2, c2) images collected at the Texas red channel; (a3, b3, and c3) overlays of the DIC and Texas red channel images; (d) average DOX fluorescence intensity determined by measuring the DOX fluorescence intensity from four different tumor regions on the tumor section; (e) total area of DOX fluorescence from four different tumor regions on the tumor section. The scale bar on all the confocal images is 20 μm.

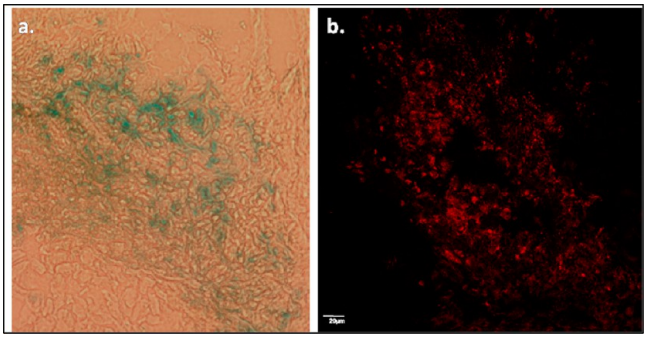

Figure 6. (a) Prussian blue staining of a tumor section demonstrating the co-localization of iron oxide nanoparticles with DOX (b). Scale bar: 20 μm.

Transfection of the Cells with Firefly Luciferase. While it was a suitable model for solid tumor penetration study, the S.C. tumor model is an approximation of ovarian cancer. In ovarian cancer patients, the absence of an anatomical barrier between the ovaries and the peritoneal cavity reduces the barrier for the metastasis, and extensive tumor nodules can be formed on the peritoneal surface by cancer cells escaped from the ovaries.[5] To closely mimic the disease, we established an I.P. disease model by injecting SKOV-3 cells intraperitoneally and evaluated the efficacy of the DOX-loaded nanoparticles accordingly.

We relied on bioluminescence imaging to monitor the growth of tumors in the peritoneal cavity and to assess the efficacy of the therapy. In order to accomplish this, SKOV-3 cells were transfected with a bioluminescence reporter, firefly luciferase, using EF1a-luciferase (firefly)-2A-RFP (blasticidin)

dx.doi.org/10.1021/am404946v | ACS Appl. Mater. Interfaces 2014, 6, 697−705

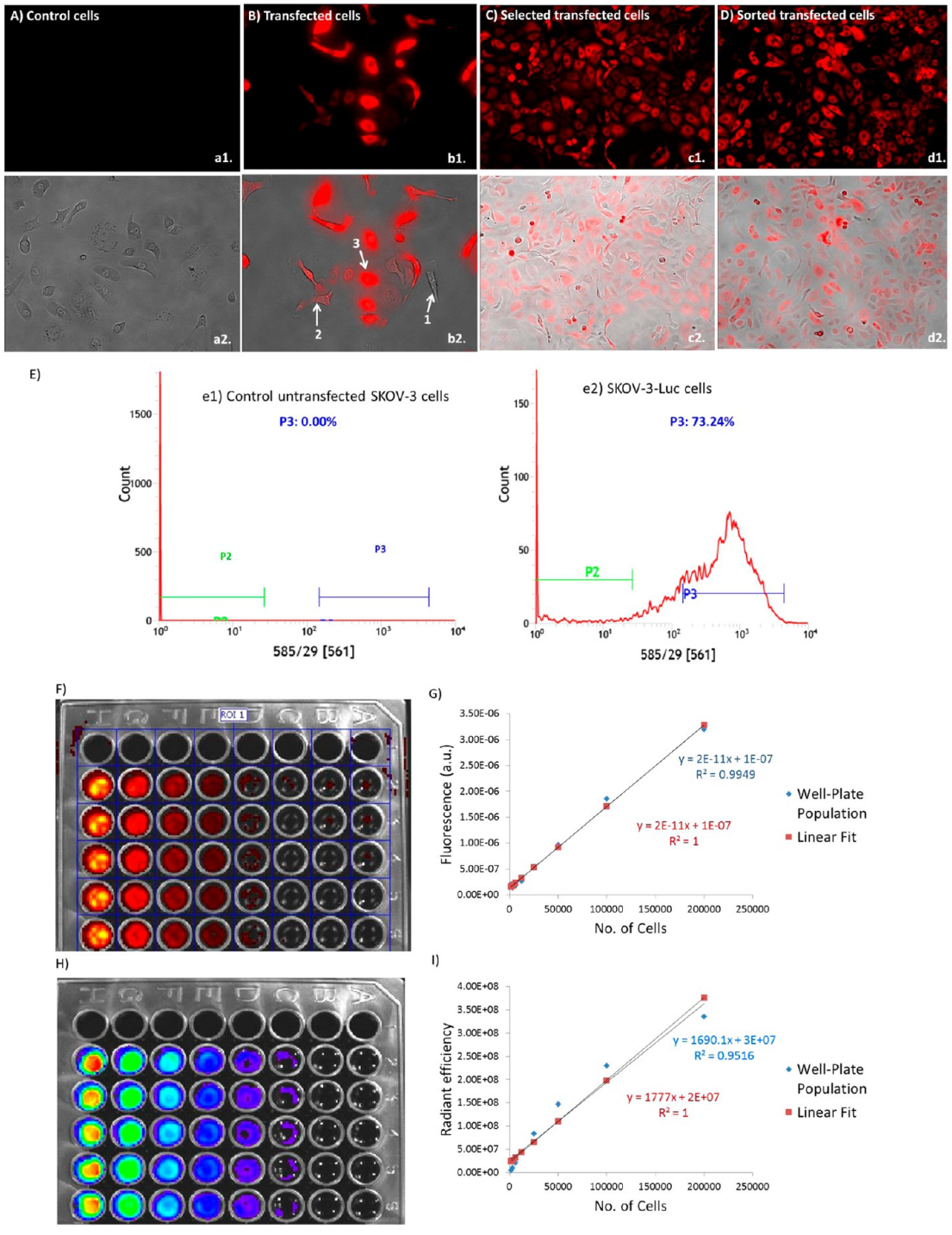

Figure 7. Transfection of SKOV-3 cancer cells with firefly luciferase and RFP. Fluorescence images collected on a fluorescence microscope for SKOV-3 cancer cells transfected with EF1a-luciferase (firefly)-2A-RFP (blasticidin) lentivirus. The red fluorescence corresponds to the expression of the RFP. (a) Control cells (no lentivirus added); (b) SKOV-3 cells transfected with lentivirus (**1** is an untransfected cell, **2** is a moderately transfected cell, and **3** is an efficiently transfected cell); (c) SKOV-3-Luc cells selected by the antibiotic blasticidin; and (d) SKOV-3-Luc cells sorted on a flow cytometer. (a1, b1, c1, and d1) fluorescent images; (a2, b2, c2, and d2) overlays of the fluorescent images and the corresponding DIC image. The magnification for parts a and b is 200×; the magnification for parts c and d is 100×. (e) Flow cytometry histograms showing the sorting of SKOV-3 cells on a flow cytometer: (e1) no cells were collected in control untransfected cells as RFP is not expressed; (e2) sorting of the SKOV-3-Luc cells. Only population 3 (P3) which represents 73% of all the cells and exhibits optimal transfection was collected and cultured for *in vivo* experiments. (f) Fluorescence image collected on the IVIS system for a 96-well plate containing a serial dilution of luciferase transfected cells ($n = 5$). (g) Quantification of the RFP fluorescence signal from the wells in part f using the LiveImage software. The fluorescence signal is linearly proportional to the number of cells. (h) Bioluminescence image collected on the IVIS system for the same 96-well plate used in part f following the addition of D-luciferin. (i) Quantification of the bioluminescence signal from part h as radiant efficiency using the LiveImage software. The bioluminescence signal is linearly proportional to the number of cells.

dx.doi.org/10.1021/am404946v | *ACS Appl. Mater. Interfaces* 2014, 6, 697−705

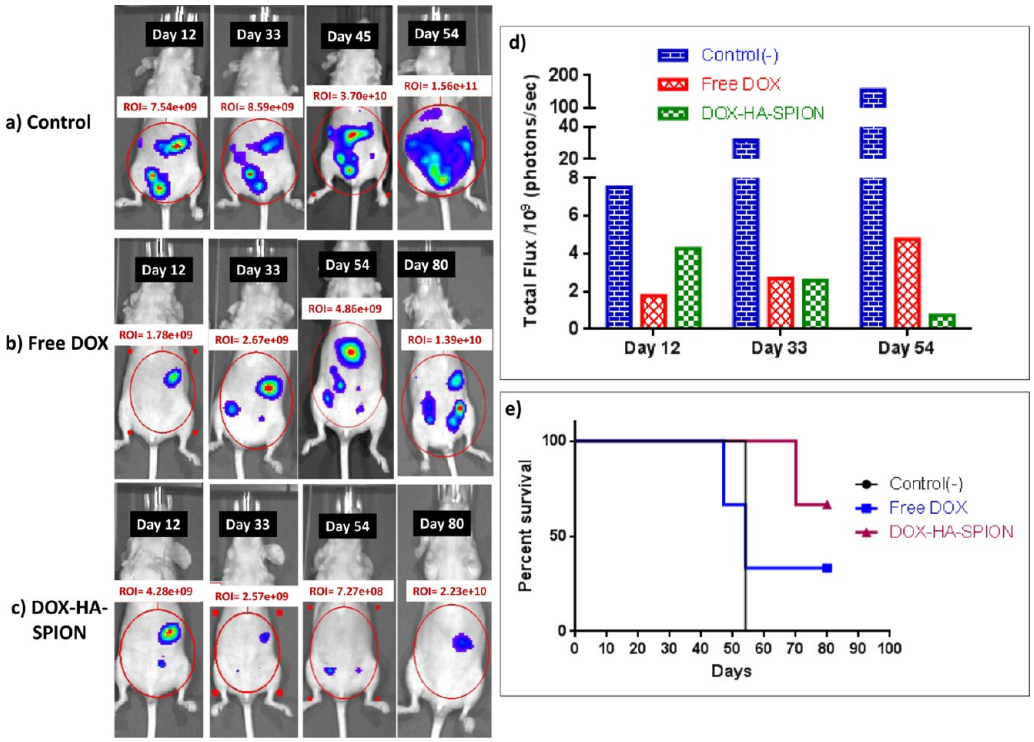

Figure 8. Bioluminescence imaging of tumor progression in mice inoculated with SKOV-3-Luc cancer cells and treated with PBS (a), free DOX (b), and DOX-HA-SPION (c). The day number in the images is the day after cell injection in the peritoneal cavity of mice. Treatment stopped at day 33 for all mice, and the progress of the disease was monitored thereafter. ROIs were drawn around the abdomens, and measurements were automatically generated as integrated flux of photons (photons/s) by the LivingImage processing software. Control mice had to be euthanized at day 54 due to excessive abdomen growth. (d) Bar graph showing the total flux of photons for the ROIs in parts a, b, and c). (e) Animal survival curve showing the number of live animals during the study.

lentivirus. The cells were incubated with the lentivirus for 72 h, and transduced cells were selected by treating the cells with the antibiotic blasticidin. The transduction process was monitored using a fluorescence microscope (Figure 7), with the expression of the red fluorescent protein (RFP) signaling successful transduction (Figure 7b). Cells that failed to express the gene (labeled 1 in Figure 7b) died, and only those with efficient transduction survived (Figure 7c). RFP expressing cells were sorted on a flow cytometer, and cells with the highest/brightest signals were collected and cultured (Figure 7d and e). The efficiency of transduction was finally assessed on the IVIS Spectrum imaging system with both bioluminescence and fluorescence imaging capabilities. Serial dilutions of the transduced cells were cultured in a 96-well black-walled, clear bottomed plate, and their fluorescence (Figure 7f) and bioluminescence images (Figure 7h) were obtained. Quantification of both the fluorescence (Figure 7g) and bioluminescent signals (Figure 7i) showed proportionality and linearity with the number of cells. The collective analysis of these results indicated that the transduction was successful and the transduced cells are suitable for *in vivo* applications.

Efficacy of the DOX-HA-SPION against the I.P. Tumor Model. It is well accepted clinically that the therapeutic index of cytotoxic drugs is increased following an I.P. administration of therapeutics compared to the I.V. route.[48] The presence of the peritoneal plasma barrier makes the peritoneal clearance of drugs much slower than plasma clearance, resulting in higher peritoneal concentrations of drugs in the vicinity of the tumors.[49] This aspect is of immense importance for effective peritoneal chemotherapy against tumors that are smaller than 1 mm. These tumors are characterized by undeveloped or absent vasculature, rendering I.V. administration of drugs inefficient. Thus, we decided to evaluate the efficacy of the I.P. route for drug administration. Three groups of mice were injected intraperitoneally with the Luc-transfected SKOV-3 cells (1×10^6 cells/mouse), and bioluminescence images were acquired following the I.P. injection of D-luciferin (150 mg/kg-body weight) to confirm the viability of cells in the mice. Treatment with either DOX or DOX-HA-SPION started the day following cell injection. A control group that received PBS was used as a negative control. The chemotherapeutic agent was administered three times per week for 4 weeks at a concentration of 2 mg-DOX/kg-body weight, which was well below the reported maximum tolerated dose of DOX in mice (8 mg-DOX/kg-body weight).[50] The weight and the abdomen size of the mice were regularly monitored, and bioluminescence images were collected weekly. In addition, diffuse light imaging tomography (DLIT) images were acquired, which combined a filtered 2D bioluminescent sequence with a surface topography to represent the bioluminescent source in a 3D space. The last treatment was administered on day 33 following cell injection, and the study was concluded on day 80 where all surviving mice were euthanized.

In general, the results from the I.P. ovarian tumor model corroborated those of the S.C. tumor model. Tumors grew uncontrollably in the control mice receiving PBS as depicted in the bioluminescence images in Figure 8a. All control mice had to be euthanized 54 days following the injection of the Luc-transfected SKOV-3 cancer cells due to significant increases in the abdomen sizes and the formation of ascites. Whereas free

dx.doi.org/10.1021/am404946v | ACS Appl. Mater. Interfaces 2014, 6, 697−705

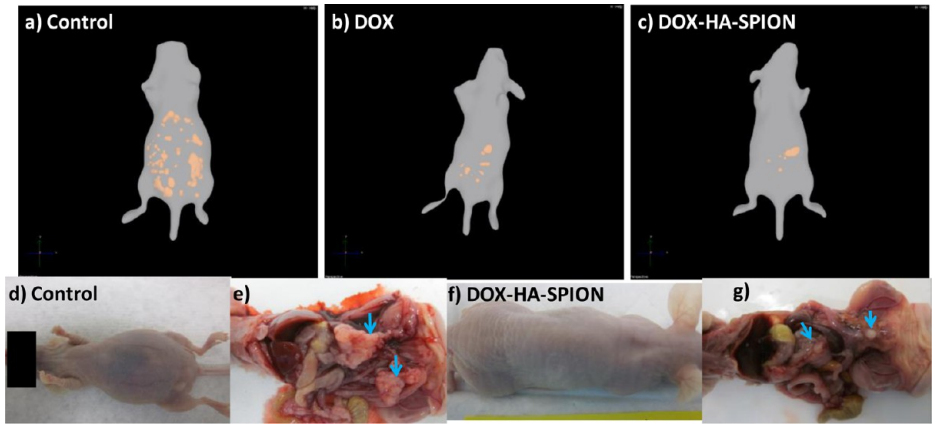

Figure 9. DLIT images showing the distribution of tumors in the peritoneal cavities of representative control (a), free DOX-treated (b), and DOX-HA-SPION-treated (c) mice at day 54 following cell injection. 3D animated videos are available in the Supporting Information. (d, e) Images of a control mouse euthanized at day 54; (f, g) images of a DOX-HA-SPION-treated mouse euthanized at day 80. The control mice exhibited an enlarged abdomen as revealed in part d due to the excessive development of ascites as a result of the uncontrolled growth of tumors (e). On the other hand, the mouse treated with the nanoparticle formulation showed regular abdomen size (f), indicating that tumor growth was under control (g). The blue arrows in parts e and g are pointing at the tumors.

DOX showed some control of tumor growth during the course of treatment, as shown in Figure 8b (days 12 and 33), tumors grew and spread in the peritoneal cavity of the mice once treatment was halted (Figure 8b, days 54 and 80, and Figure 8d). Out of three DOX-treated mice, one was found dead and another was euthanized on day 47 following cell injection due to extreme weight loss. The third mouse survived until the end of the study (Figure 8e). On the other hand, DOX delivered by SPION not only caused tumor regression during treatment (Figure 8c, days 12 and 33) but also prevented tumor growth long after the final nanoparticle injection, as shown in Figure 8c (day 54) and d. In fact, all mice receiving the nanoparticle formulation survived without signs of adverse health effects until day 70 when the first mouse had to be euthanized due to enlarged abdomen and ascite accumulation. The other two mice survived until the end of the study at day 80 (Figure 8e). Bioluminescence images collected on day 80 showed the little signs of the tumors. Despite its benefits, the I.P. administration of DOX still holds significant risk in terms of off-site toxicity. It has been shown clinically that I.P. chemotherapy resulted in significantly greater bone marrow, renal, gastrointestinal, and neurological toxicities when compared to I.V. chemotherapy, while reducing the quality of life of patients.[51] In addition, the higher concentrations of drugs in I.P. dialysate do not mirror the drug levels in the tumors because drugs such as cisplatin do not penetrate more than 1−2 mm following an I.P. injection.[52] These facts may explain the early mortality and the moderate therapeutic outcome in the mice receiving free DOX. On the other hand, conjugating DOX onto SPION alters the pharmacokinetic and pharmacodynamic properties of the drug. We have shown previously that free DOX and DOX-HA-SPIONs exhibited different uptake mechanisms and cellular distributions, and acted against different cellular targets. While free DOX localized prominently in the nucleus upon incubation with SKOV-3 cells, DOX-HA-SPION was dispersed in the cytoplasm targeting the mitochondria while slowly releasing DOX to affect its targets in the nucleus.[27] In addition, the HA coating on the nanoparticles can assist the delivery of DOX deeper in the tumor mass through receptor mediated transcytosis, thus causing a larger population of tumor cells to be subjected to the drug.[42]

The overall therapeutic benefit of the DOX-loaded nanoparticles was further supported by bioluminescence animations reconstructed from DLIT images. Figure 9 shows the distribution of tumors (shown as brown objects) in the peritoneal cavity of mice. It is clear that the mice treated with DOX loaded on nanoparticles exhibited much less tumors compared to the control mice and the free DOX-treated mice (3D video animations of the images in Figure 8 are provided in the Supporting Information). The dissection of control mice showed the presence of large tumors in the peritoneal cavity. On the other hand, far fewer tumors were found in the peritoneal cavity of DOX-HA-SPION-treated mice, corroborating the results of the bioluminescence imaging.

CONCLUSION

Consistent with our previous *in vitro* studies, we have established that HA-coated iron oxide nanoparticles can enhance the efficacy of chemotherapeutic drugs such as DOX in two mouse ovarian cancer models. Compared with the free drug, DOX delivered by HA nanoparticles accumulated in tumors in much higher quantities and was distributed in much larger areas in tumor tissues. In addition, the magnetic properties of the nanoparticles enabled non-invasive monitoring of nanoparticle delivery via MRI. Thus, the HA functionalized iron oxide nanoparticles are an attractive theranostic platform to target CD44 expressing tumors.

ASSOCIATED CONTENT

Supporting Information

3D video animations of tumor bearing mice with and without treatments. am404946v_si_002.avi: Mice treated with Dox-NP. am404946v_si_003.avi: Mice treated with Dox only. am404946v_si_004.avi: Mice without any treatment. This material is available free of charge via the Internet at http://pubs.acs.org.

AUTHOR INFORMATION

Corresponding Authors

*E-mail: m.eldakdouki@bau.edu.lb; eldakdouki@chemistry.msu.edu.
*E-mail: xuefei@chemistry.msu.edu.

Notes

The authors declare no competing financial interest.

■ ACKNOWLEDGMENTS

This work was supported by the National Institutes of Health (R01CA149451) (X.H.). We would like to thank the Department of Radiology, Michigan State University, for the very generous support toward access of the MRI scanner.

■ REFERENCES

(1) American Cancer Society. *Cancer Facts & Figures 2013*; American Cancer Society: Atlanta, GA, 2013.
(2) Dinh, P.; Harnett, P.; Piccart-Gebhart, M. J.; Awada, A. *Crit. Rev. Oncol. Hematol.* **2008**, *67*, 103−112.
(3) Ozols, R. F.; Bundy, B. N.; Greer, B. E.; Fowler, J. M.; Clarke-Pearson, D.; Burger, R. A.; Mannel, R. S.; de Geest, K.; Hartenbach, E. M.; Baergen, R. *J. Clin. Oncol.* **2003**, *21*, 3194−3200.
(4) Kalachand, R.; Hennessy, B. T.; Markman, M. *Drugs* **2011**, *71*, 947−967.
(5) Bast, R. C.; Hennessy, B.; Mills, G. B. *Nat. Rev. Cancer* **2009**, *9*, 415−428.
(6) Goff, B. A.; Mandel, L.; Muntz, H. G.; Melancon, C. H. *Cancer* **2000**, *89*, 2068−2075.
(7) Gore, M. E.; Fryatt, I.; Wiltshaw, E.; Dawson, T. *Gynecol. Oncol.* **1990**, *36*, 207−211.
(8) Poveda, A.; Vergote, I.; Tjulandin, S.; Kong, B.; Roy, M.; Chan, S.; Filipczyk-Cisarz, E.; Hagberg, H.; Kaye, S. B.; Colombo, N.; Lebedinsky, C.; Parekh, T.; Gomez, J.; Park, Y. C.; Alfaro, V.; Monk, B. J. *Ann. Oncol.* **2011**, *22*, 39−48.
(9) de Placido, S.; Scambia, G.; di Vagno, G.; Naglieri, E.; Lombardi, A. V.; Biamonte, R.; Marinaccio, M.; Carteni, G.; Manzione, L.; Febbraro, A.; de Matteis, A.; Gasparini, G.; Valerio, M. R.; Danese, S.; Perrone, F.; Lauria, R.; de Laurentiis, M.; Greggi, S.; Gallo, C.; Pignata, S. *J. Clin. Oncol.* **2004**, *22*, 2635−2642.
(10) Welch, S. A.; Hirte, H. W.; Elit, L.; Schilder, R. J.; Wang, L.; Macalpine, K.; Wright, J. J.; Oza, A. M. *Int. J. Gynecol. Cancer* **2010**, *20*, 787−793.
(11) Wagner, U.; du Bois, A.; Pfisterer, J.; Huober, J.; Loibl, S.; Lueck, H.-J.; Sehouli, J.; Gropp, M.; Staehle, A.; Schmalfeldt, B.; Meier, W.; Jackisch, C. *Gynecol. Oncol.* **2007**, *105*, 132−137.
(12) Agarwal, R.; Kaye, S. B. *Nat. Rev. Cancer* **2003**, *3*, 502−516.
(13) Yap, T. A.; Carden, C. P.; Kaye, S. B. *Nat. Rev. Cancer* **2009**, *9*, 167−181.
(14) Banerjee, S.; Gore, M. *Oncologist* **2009**, *14*, 706−716.
(15) van der Bilt, A. R. M.; de Vries, E. G. E.; de Jong, S.; Timmer-Bosscha, H.; van der Zee, A. G. J.; Reyners, A. K. L. *Crit. Rev. Oncol. Hematol.* **2012**, *84*, 224−242.
(16) Markman, M.; Sehouli, J.; Levenback, C. F.; Chi, D. S. *J. Oncol.* **2010**, *2010*, 171425.
(17) Kanwar, J. R.; Sun, X.; Punj, V.; Sriramoju, B.; Mohan, R. R.; Zhou, S.-F.; Chauhan, A.; Kanwar, R. K. *Nanomedicine* **2012**, *8*, 399−414.
(18) Moghimi, S. M. *Nanomedicine* **2011**, *7*, 515−518.
(19) Baker, M. *Nat. Methods* **2010**, *7*, 957−962.
(20) Lammers, T.; Rizzo, L. Y.; Storm, G.; Kiessling, F. *Clin. Cancer Res.* **2012**, *18*, 4889−4894.
(21) Huang, Y.; He, S.; Cao, W.; Cai, K.; Liang, X.-J. *Nanoscale* **2012**, *4*, 6135−6149.
(22) Ma, P.; Mumper, R. J. *Nano Today* **2013**, *8*, 313−331.
(23) Ferrari, M. *Nat. Rev. Cancer* **2005**, *5*, 161−171.
(24) Bu, H. H.; Gao, Y.; Li, Y. P. *Sci. China: Chem.* **2010**, *53*, 2226−2232.
(25) El-Dakdouki, M. H.; El-Boubbou, K.; Zhu, D. C.; Huang, X. *RSC Adv.* **2011**, *1*, 1449−1452.
(26) El-boubbou, K.; Gruden, C.; Huang, X. *J. Am. Chem. Soc.* **2007**, *129*, 13392−13393.
(27) El-Dakdouki, M. H.; Zhu, D. C.; El-Boubbou, K.; Kamat, M.; Chen, J.; Li, W.; Huang, X. *Biomacromolecules* **2012**, *13*, 1144−1151.
(28) El-boubbou, K.; Zhu, D. C.; Vasileiou, C.; Borhan, B.; Prosperi, D.; Li, W.; Huang, X. *J. Am. Chem. Soc.* **2010**, *132*, 4490−4499.
(29) El-Dakdouki, M. H.; El-Boubbou, K.; Kamat, M.; Huang, R.; Abela, G. S.; Kiupel, M.; Zhu, D. C.; Huang, X. *Pharm. Res.* **2013**, DOI: 10.1007/s11095-013-1021-8.
(30) Li, H.; El-Dakdouki, H.; Zhu, D. C.; Abela, G. S.; Huang, X. *Chem. Commun.* **2012**, *48*, 3385−3387.
(31) Kamat, M.; El-Boubbou, K.; Zhu, D. C.; Lansdell, T.; Lu, X.; Li, W.; Huang, X. *Bioconjugate Chem.* **2010**, *21*, 2128−2135.
(32) Kouyoumdjian, H.; Zhu, D. C.; El-Dakdouki, M. H.; Lorenz, K.; Chen, J.; Li, W.; Huang, X. *ACS Chem. Neurosci.* **2013**, *4*, 575−584.
(33) Prayer, L.; Stiglbauer, R.; Kramer, J.; Wimberger, D.; Poelzleitner, D.; Schima, W.; Kainz, C.; Koelbl, H.; Haugen, I.; Imhof, H. *Br. J. Radiol.* **1993**, *66*, 415−419.
(34) Yigit, M. V.; Moore, A.; Medarova, Z. *Pharm. Res.* **2012**, *29*, 1180−1188.
(35) Zhao, Z.; Zhou, Z.; Bao, J.; Wang, Z.; Hu, J.; Chi, X.; Ni, K.; Wang, R.; Chen, X.; Chen, Z.; Gao, J. *Nat. Commun.* **2013**, DOI: 10.1038/ncomms3266.
(36) Lee, N.; Hyeon, T. *Chem. Soc. Rev.* **2012**, *41*, 2575−2589.
(37) Chen, B.; Sun, Q.; Wang, X.; Gao, F.; Dai, Y.; Yin, Y.; Ding, J.; Gao, C.; Cheng, J.; Li, J.; Sun, X.; Chen, N.; Xu, W.; Shen, H.; Liu, D. *Int. J. Nanomed.* **2008**, *3*, 277−286.
(38) Li, K.; Chen, B.; Xu, L.; Feng, J.; Xia, G.; Cheng, J.; Wang, J.; Gao, F.; Wang, X. *Int. J. Nanomed.* **2013**, *8*, 1867−1877.
(39) Chen, B.; Cheng, J.; Wu, Y.; Gao, F.; Xu, W.; Shen, H.; Ding, J.; Gao, C.; Sun, Q.; Sun, X.; Cheng, H.; Li, G.; Chen, W.; Chen, N.; Liu, L.; Li, X.; Wang, X. *Int. J. Nanomed.* **2009**, *4*, 73−78.
(40) Jiang, Z.; Chen, B.-A.; Xia, G.-H.; Wu, Q.; Zhang, Y.; Hong, T.-Y.; Zhang, W.; Cheng, J.; Gao, F.; Liu, L.-J.; Li, X.-M.; Wang, X.-M. *Int. J. Nanomed.* **2009**, *4*, 107−114.
(41) El-Dakdouki, M. H.; Pure, E.; Huang, X. *Nanoscale* **2013**, *5*, 3895−3903.
(42) El-Dakdouki, M. H.; Pure, E.; Huang, X. *Nanoscale* **2013**, *5*, 3904−3911.
(43) Na, H. B.; Song, I. C.; Hyeon, T. *Adv. Mater.* **2009**, *21*, 2133−2148.
(44) Seymour, L. W.; Ulbrich, K.; Strohalm, J.; Kopecek, J.; Duncan, R. *Biochem. Pharmacol.* **1990**, *39*, 1125−1131.
(45) Lee, C. C.; Gillies, E. R.; Fox, M. E.; Guillaudeu, S. J.; Frechet, J. M. J.; Dy, E. E.; Szoka, F. C. *Proc. Natl. Acad. Sci. U.S.A.* **2006**, *103*, 16649−16654.
(46) Minchinton, A. I.; Tannock, I. F. *Nat. Rev. Cancer* **2006**, *6*, 583−592.
(47) Primeau, A. J.; Rendon, A.; Hedley, D.; Lilge, L.; Tannock, I. F. *Clin. Cancer Res.* **2005**, *11*, 8782−8788.
(48) Ceelen, W. P.; Flessner, M. F. *Nat. Rev. Clin. Oncol.* **2010**, *7*, 108−115.
(49) Markman, M. *Int. J. Gynecol. Cancer* **2008**, *18* (Suppl. 1), 33−35.
(50) Boven, E.; Schluper, H. M. M.; Erkelens, C. A. M.; Pinedo, H. M. *Eur. J. Cancer* **1990**, *26*, 983−986.
(51) Gore, M.; du Bois, A.; Vergote, I. *J. Clin. Oncol.* **2006**, *24*, 4528−4530.
(52) Vergote, I.; Amant, F.; Leunen, K.; Cadron, I.; Van Gorp, T.; Neven, P.; Berteloot, P. *Oncologist* **2008**, *13*, 410−414.